



ELSEVIER

1 January 1998

OPTICS
COMMUNICATIONS

Optics Communications 145 (1998) 195–202

Full length article

Thin grating sequential diffractions for the analysis of Bragg diffractions by superimposed transmission phase gratings

Michael R. Wang^{a,1}, Bing Chen^b^a *Department of Electrical and Computer Engineering, University of Miami, Coral Gables, FL 33124, USA*^b *New Span Opto-Technology Inc., Miami, FL, USA*

Received 4 December 1996; revised 5 August 1997; accepted 5 August 1997

Abstract

We present a thin grating sequential diffraction technique on analyzing Bragg diffractions by superimposed transmission phase gratings. It can account for diffractions by any number of superimposed gratings with symmetric and asymmetric diffraction geometries. The angular and wavelength selectivity curves are found to depart from the $(\text{sinc})^2$ functional dependence of single-grating diffraction cases owing to the energy coupling among all diffracted and undiffracted beams. The calculation results match well with those calculated using thin-grating decomposition technique. The simple computation technique should be suitable for design engineers to establish grating index combinations prior to experimental implementation of optical beam splitting components. © 1998 Elsevier Science B.V.

Keywords: Grating; Superimposed; Diffraction; Beam splitting; Fanout; Interconnection

1. Introduction

Bragg diffractions by superimposed transmission phase gratings are important schemes for the realization of optical beam splitters for optical fanout interconnection, neural network implementation, data storage, and parallel optical processing and computing. The theory of optical beam diffractions by superimposed transmission phase gratings has been developed by several authors [1–7]. One of the first analyses was given by Alferness and Case [1,2] with a thin grating decomposition technique that describes each partitioned thin grating with a transmittance function and then calculates the overall transmittance function of the thick grating. Their analysis is limited to TE (transverse electric) polarized waves and is not suitable for 3-D diffractions. Coupled-wave approach is an excellent technique for analyzing Bragg diffractions by superimposed planar phase gratings in a common diffraction plane (2-D diffraction) [3–5]. The formulations are relatively simple

to examine 2-D diffraction problems since TE and TM (transverse magnetic) beam polarizations can be separately treated. For a 3-D diffraction by superimposed planar phase gratings, complete modal analysis [6,7] yields complicated results, because the grating vector can have an arbitrary orientation with respect to the plane of incidence. As a consequence the TE and TM incident field components become coupled inside the grating region and can no longer be treated separately as in the 2-D case. The coupled diffraction by superimposed gratings makes the situation more complicated than single grating 3-D diffractions [8,9]. Recently, two powerful computation techniques, namely multiple-scattering theory [10,11] and beam propagation method (BPM) [12,13], have been used to analyze superimposed grating diffraction problems. Both the multiple-scattering theory and the BPM can account for arbitrary grating angle separations and Bragg conditions. However, the multiple-scattering theory suffers from numerical problems when the number of gratings increases [12]. It is also restricted to two-dimensional diffraction situations. Large angle BPM for three-dimensional superimposed grating diffraction is not yet available. It is, so

¹ Corresponding author. E-mail: mawang@eng.miami.edu.

far, hard for a design engineer to determine suitable grating index combinations prior to device implementation. As a result, superimposed gratings are often recorded through trial and error in hoping on getting a desired energy distributions for fanout diffracted beams.

We describe here a simple numerical computation method, namely thin grating sequential diffraction technique, for analyzing Bragg diffractions by superimposed transmission phase gratings. We address in this paper again diffractions in 2-D geometry that show the simplicity and validity of the concept. Discussion on 3-D diffractions that incorporate the thin grating sequential diffraction technique and the 3-D diffraction theory [9] will be reported elsewhere. Superimposed planar phase gratings are partitioned into grating subsections with each grating subsection still consisting of superimposed planar phase gratings. The Bragg diffraction of an incoming coherent collimated light beam in the grating subsection is calculated sequentially by each grating using the coupled-wave theory [9,14]. In other words, we calculate the Bragg diffraction of both TE and TM polarizations by one grating of the subsection length. The results of this grating subsection diffraction are used as incident beams to calculate diffraction by another superimposed grating in the same grating subsection, and so on. After all superimposed gratings have been considered for diffractions in the same grating subsection, the overall results are used as incident beams for the next grating subsection diffractions. Again the diffraction calculation is performed sequentially for all superimposed gratings in the subsection. The calculations go on until all grating subsections have been considered.

Because the grating subsection length is small, the sequence of grating diffraction by the superimposed gratings in each subsection is no longer important. Thus, the technique shows validity on analyzing both direct coupled

and cross coupled diffraction cases. The numerical computation technique is described in detail below. Calculations demonstrate the energy coupling among all diffracted beams. The validity of the technique is discussed. Guidelines on establishing a uniform diffraction efficiency for all diffracted beams for beam splitting are also provided. Also considered are the subsection grating size to the computation error, the effects of detuning from the Bragg condition, and the resultant angular and wavelength selectivities.

2. Thin grating sequential diffraction technique

The numerical calculation of the Bragg diffractions by superimposed transmission phase gratings is based on the well known coupled wave diffraction theory [14] for single grating with the thin grating sequential diffraction technique introduced herein.

Fig. 1 shows the diffraction geometry of a single grating that has been partitioned into several grating subsections. Incident angle α , diffraction angle α_d , grating thickness d , and grating fringe orientation are defined. The grating can be described by a periodic index of refraction:

$$n = n_0 + \Delta n \cos(\mathbf{K} \cdot \mathbf{r}), \quad (1)$$

where n_0 is the bulk index and Δn is the sinusoidal grating index modulation with $\Delta n \ll n_0$. \mathbf{K} is the grating vector. \mathbf{k} and \mathbf{k}_d as shown in Fig. 1 are the incident and diffracted beam propagation vectors, respectively. For the superimposed grating case, the second term becomes $\sum_{i=1}^m \Delta n_i \cos(\mathbf{K}_i \cdot \mathbf{r})$ with m the total grating number and subscript i designating the particular grating.

From the coupled wave diffraction theory [9,14] we obtain the weighting factors of the Bragg diffraction that relate the diffracted and undiffracted beam amplitudes with

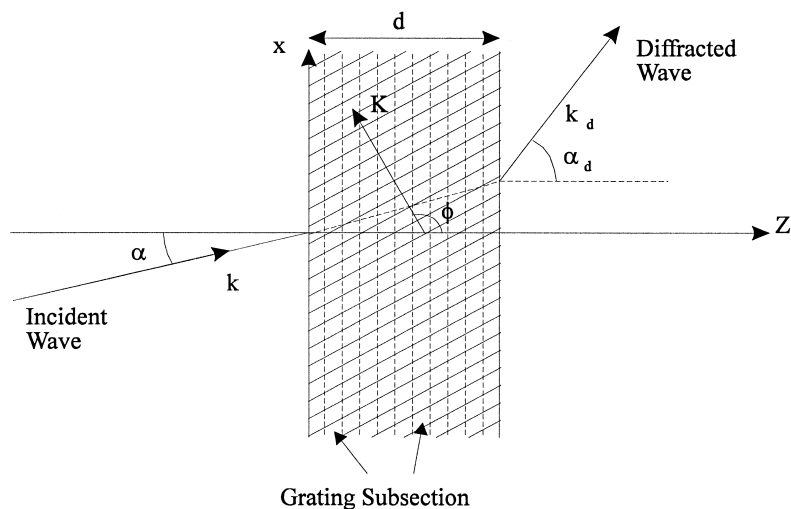


Fig. 1. Model of a Bragg transmission phase grating with slanted grating fringes and an oblique incident angle.

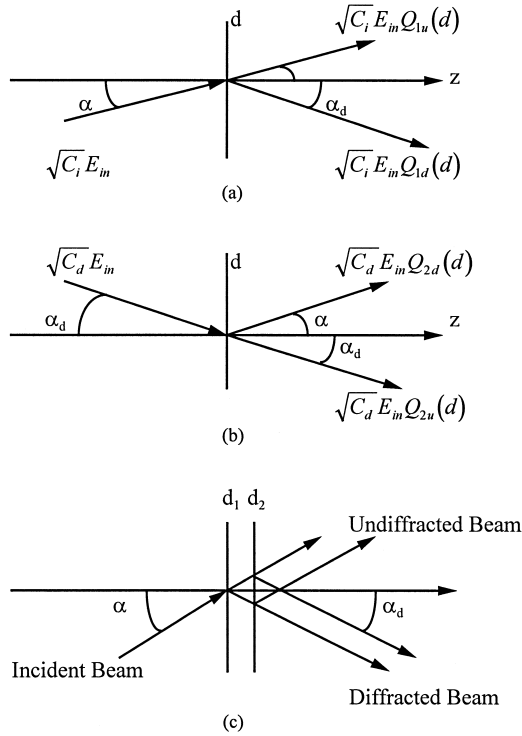


Fig. 2. Definition of weighting factors (a) Q_{1u} and Q_{1d} at incident angle α and (b) Q_{2u} and Q_{2d} at incident angle α_d , (c) origin of the total diffracted and undiffracted beam amplitudes.

that of the incident beam, as shown in Fig. 2. For beam incidence at angle of α (see Fig. 2(a)), the two weighting factors $Q_{1u}(d)$ and $Q_{1d}(d)$ are [15]

$$Q_{1u}(d) = \exp\left(-j\frac{\vartheta}{2C_d}d\right) \cos\left(\frac{1}{2}\left(\frac{\vartheta^2}{C_d^2} + \frac{4\kappa'^2}{C_i C_d}\right)^{1/2}d\right) + \frac{j\vartheta}{C_d\left(\vartheta^2/C_d^2 + 4\kappa'^2/C_i C_d\right)^{1/2}} \times \exp\left(-j\frac{\vartheta}{2C_d}d\right) \sin\left(\frac{1}{2}\left(\frac{\vartheta^2}{C_d^2} + \frac{4\kappa'^2}{C_i C_d}\right)^{1/2}d\right), \quad (2)$$

$$Q_{1d}(d) = -\frac{j2\kappa'}{(C_i C_d)^{1/2}\left(\vartheta^2/C_d^2 + 4\kappa'^2/C_i C_d\right)^{1/2}} \times \exp\left(-j\frac{\vartheta}{2C_d}d\right) \sin\left(\frac{1}{2}\left(\frac{\vartheta^2}{C_d^2} + \frac{4\kappa'^2}{C_i C_d}\right)^{1/2}d\right). \quad (3)$$

Similarly, for incident angle α_d as shown in Fig. 2(b), where the incident and diffracted beams are interchanged,

a new set of weighting factors, $Q_{2u}(d)$ and $Q_{2d}(d)$, are given as [15]

$$Q_{2u}(d) = \exp\left(-j\frac{\vartheta}{2C_d}d\right) \cos\left(\frac{1}{2}\left(\frac{\vartheta^2}{C_d^2} + \frac{4\kappa'^2}{C_i C_d}\right)^{1/2}d\right) - \frac{j\vartheta}{C_d\left(\vartheta^2/C_d^2 + 4\kappa'^2/C_i C_d\right)^{1/2}} \exp\left(-j\frac{\vartheta}{2C_d}d\right) \times \sin\left(\frac{1}{2}\left(\frac{\vartheta^2}{C_d^2} + \frac{4\kappa'^2}{C_i C_d}\right)^{1/2}d\right), \quad (4)$$

$$Q_{2d}(d) = -\frac{j2\kappa'}{(C_i C_d)^{1/2}\left(\vartheta^2/C_d^2 + 4\kappa'^2/C_i C_d\right)^{1/2}} \times \exp\left(-j\frac{\vartheta}{2C_d}d\right) \sin\left(\frac{1}{2}\left(\frac{\vartheta^2}{C_d^2} + \frac{4\kappa'^2}{C_i C_d}\right)^{1/2}d\right), \quad (5)$$

where

$$\kappa' = \begin{cases} \kappa & \text{for s-polarized (TE) wave} \\ \kappa(\hat{k} \cdot \hat{k}_d) & \text{for p-polarized (TM) wave} \end{cases} \quad (6)$$

and

$$k = \frac{\pi \Delta n}{\lambda}, \quad (7)$$

$$C_i = \cos \alpha, \quad (8)$$

$$C_d = \cos \alpha_d. \quad (9)$$

Here an s-polarized (TE) wave defines an incident beam whose polarization is perpendicular to the incident plane, whereas the p-polarized (TM) wave has a polarization parallel to the plane. \hat{k} and \hat{k}_d are unit vectors of \mathbf{k} and \mathbf{k}_d , respectively. The dephasing constant ϑ is expressed as

$$\vartheta = -\frac{K^2}{4\pi n_0} \lambda \pm K \cos(\phi - \alpha), \quad \phi - \alpha < 90^\circ (> 90^\circ), \quad (10)$$

and is used to characterize the response of diffracted and undiffracted waves to slight variations in incident angle or beam wavelength near the Bragg condition ($\vartheta = 0$).

At Bragg condition, the plane wave diffraction from a transmission grating can be considered as successive diffractions from many grating subsections partitioned from the thick grating. The validity of this argument is the basis of the grating partitioning in the following numerical computation. This statement requires that for a plane-wave diffraction in a grating of interaction length ($d_1 + d_2$) the diffraction from such length equals that of successive diffractions from gratings of length d_1 and then d_2 , as

shown in Fig. 2(c). The following amplitude relationships are thus expected:

$$Q_{1u}(d_1 + d_2) = Q_{1u}(d_1)Q_{1u}(d_2) + Q_{1d}(d_1)Q_{2d}(d_2), \quad (11a)$$

$$Q_{1d}(d_1 + d_2) = Q_{1d}(d_1)Q_{2u}(d_2) + Q_{1u}(d_1)Q_{1d}(d_2). \quad (11b)$$

These relationships can be confirmed by using Eqs. (2), (3), (4), and (5). The results suggest that it is possible to divide the grating into many subsections, with the diffraction from each subsection calculated with the plane-wave theory and the total grating diffraction considered as the cumulative effect from all these subsections. As long as the total grating diffraction meets the Bragg condition with no higher diffraction orders, the grating partitioning process can allow subsection grating lengths to be smaller than that required by Bragg condition and still not considering higher diffraction orders for overall Bragg diffraction calculation purposes.

Using the single grating partitioning technique, superimposed transmission phase gratings can similarly be partitioned into many subsections and analyzed using the thin grating sequential diffraction technique. It is not straightforward to show that the superimposed-grating coupled-wave equations [3,5] can support the partitioned grating calculations that are conceptually similar to the single-grating case of Fig. 2(c) and Eq. (11). If we assume the superimposed-grating coupled-wave equations do support the partitioned grating calculations, the equations by themselves are found to support the thin grating sequential diffraction processes using single-grating coupled-wave equations when we let the grating interaction length approach zero (see Ref. [3]). With this in mind the validation of our thin grating sequential diffraction technique, restricted to the well separated Bragg diffraction angles, will be accomplished by comparing our calculation results with those calculated with a well established theory.

For the partitioned gratings each grating subsection length is small but contains all superimposed gratings. For a direct coupled case, an incident collimated beam with field amplitude E_i is propagating in the direction of the common undiffracted beam. The beam is first diffracted by grating #1 described by the single-grating diffraction theory (coupled-wave theory) [9,14,15]. The resulting diffracted beams with field amplitudes E_{d1} and E_u are now considered as incident beams to be diffracted by grating #2 in the same grating subsection. E_{d1} is the diffracted beam field amplitude of grating #1 and E_u is the undiffracted beam field amplitude. Similar subscript definition applies to following discussions. Only E_u is now diffracted by grating #2. The output fields are E_{d1} , E_{d2} , and E_u . E_{d1} is not affected by grating #2. This is based on the assumption that the Bragg angles are made sufficiently different so that there is no overlap of the angular regions of the diffracted beams. E_{d1} , E_{d2} , and E_u are now consid-

ered as incident beams for the same grating subsection for grating #3 where E_u is diffracted and E_{d1} and E_{d2} are not affected. The sequential diffractions using the single-grating diffraction theory go on until all gratings have been considered in the grating subsection. The results from the first grating subsection diffractions with field amplitudes of E_{d1} , E_{d2} , E_{d3} , ..., E_{dn} , and E_u are now the incident fields for the second grating subsection diffractions. This time both E_{d1} and E_u are diffracted by grating #1 to yield new E_{d1} and E_u and both E_{d2} and E_u are diffracted by grating #2 to yield new E_{d2} and E_u , and so on. All four weighting factors are used for the computations. The results of second grating subsection diffractions, E_{d1} , E_{d2} , E_{d3} , ..., E_{dn} , and E_u , are the incident fields for the third grating subsection. The process continues until all grating subsections have been considered for the diffraction computations. The computation equations for diffractions in any grating subsection are as follows.

Diffraction by grating #1:

$$E_1(z + \Delta d) = Q_{1u1}(\Delta d)E_u(z) + Q_{2d1}(\Delta d)E_{d1}(z), \quad (12a)$$

$$E_{d1}(z + \Delta d) = Q_{1d1}(\Delta d)E_u(z) + Q_{2u1}(\Delta d)E_{d1}(z). \quad (12b)$$

Diffraction by grating #2:

$$E_2(z + \Delta d) = Q_{1u2}(\Delta d)E_1(z + \Delta d) + Q_{2d2}(\Delta d)E_{d2}(z), \quad (13a)$$

$$E_{d2}(z + \Delta d) = Q_{1d2}(\Delta d)E_1(z + \Delta d) + Q_{2u2}(\Delta d)E_{d2}(z). \quad (13b)$$

Diffraction by grating #n:

$$E_n(z + \Delta d) = Q_{1un}(\Delta d)E_{n-1}(z + \Delta d) + Q_{2dn}(\Delta d)E_{dn}(z), \quad (14a)$$

$$E_{dn}(z + \Delta d) = Q_{1dn}(\Delta d)E_{n-1}(z + \Delta d) + Q_{2un}(\Delta d)E_{dn}(z). \quad (14b)$$

The incident beams are located at z and Δd is the grating subsection length. E_1 to E_n are intermediate calculation results of E_u . After completing all diffraction processes in the grating subsection, we have $E_{d1}(z + \Delta d)$, $E_{d2}(z + \Delta d)$, ..., $E_{dn}(z + \Delta d)$, and $E_u(z + \Delta d)$. Here, $E_u(z + \Delta d)$ equals $E_n(z + \Delta d)$. The results can be used for next grating subsection diffraction calculations.

Upon considering the diffractions by all grating subsections, the diffraction efficiencies for diffracted beams can be evaluated by dividing the diffracted beam energies by the incident beam energy as

$$\eta_n = \frac{|E_{dn}|^2}{|E_{in}|^2}, \quad (15)$$

where subscript n designates the n th diffracted beam.

The above equations apply also to cross coupled diffraction cases by only specifying that the incident beam

is propagating in the direction of one of the above diffracted beams rather than in the direction of the common undiffracted beam. The energy couples from the incident beam to E_u and then couples to other diffracted beams from E_u . The computation process is identical except the input condition.

3. Results of superimposed grating diffractions

To examine the validity of using the thin grating sequential diffraction technique for analyzing the Bragg

diffractions by superimposed transmission phase gratings, we computed the diffractions by two superimposed transmission phase gratings under the same diffraction parameters of Ref. [2] for direct coupling case. The incident angle α for TE polarized beam was set at -2° and the laser wavelength λ was $0.488 \mu\text{m}$. The bulk index n_0 was 1.52 and the total grating interaction length was $15.9 \mu\text{m}$. The diffraction angles α_d for the first and second gratings were 19.6° and -18.6° , respectively. The grating index modulation Δn_1 for the first grating was set at 0.01489 which is required to achieve 100% efficiency for its single grating diffraction case. The grating index modulation Δn_2 for the

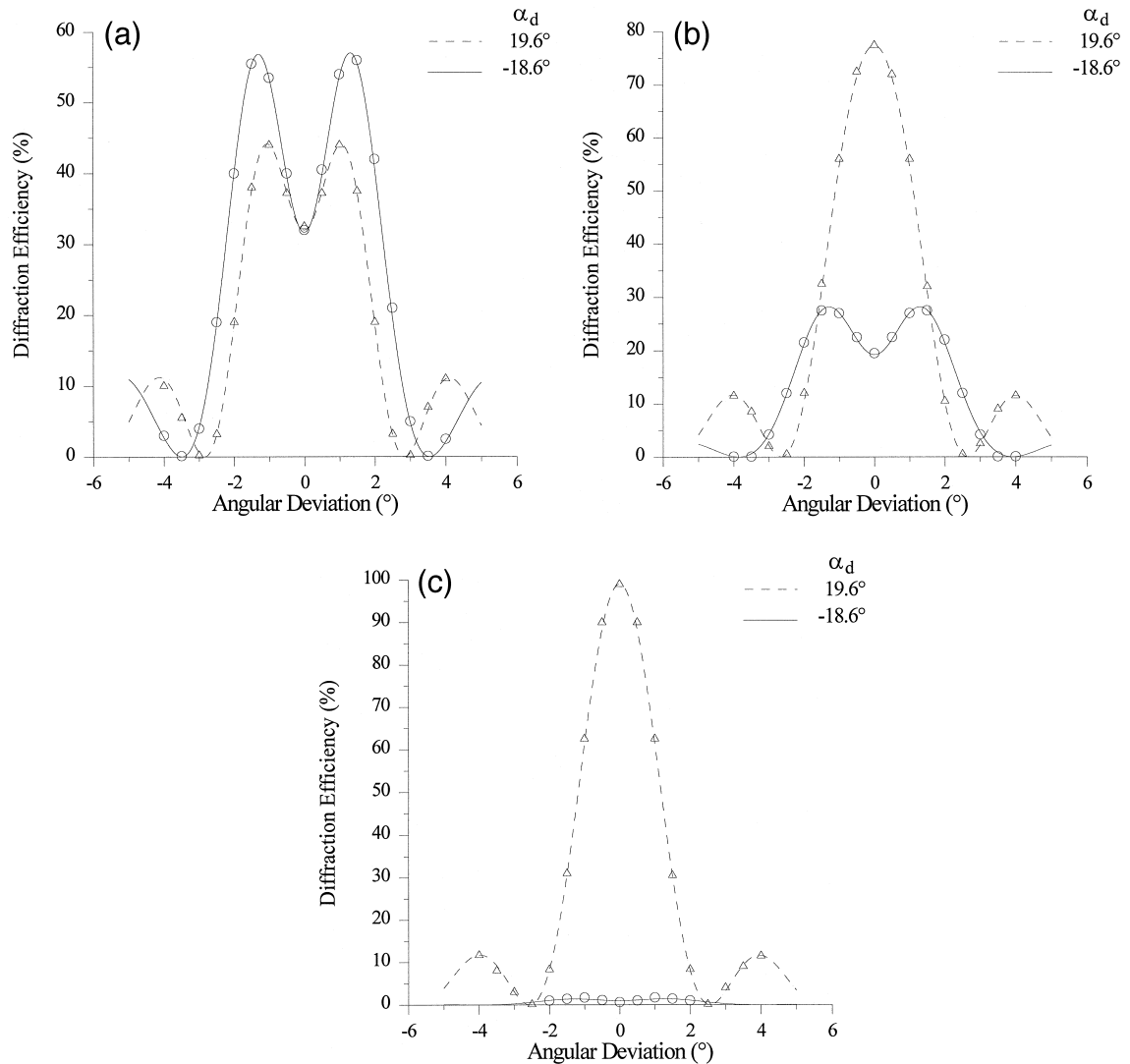


Fig. 3. Calculated angular selectivity curves for direct-coupled superimposed two-grating diffraction case of Ref. [2]. For the calculation, we used incident angle of -2° , laser wavelength of $0.488 \mu\text{m}$, TE beam polarization, bulk index of 1.52, total grating length of $15.9 \mu\text{m}$, first grating diffraction angle of 19.6° , and second grating diffraction angle of -18.6° . The first grating index Δn_1 was set at 0.01489 required for 100% of its single-grating diffraction. The second grating index Δn_2 was set at (a) $\Delta n_2 = \Delta n$, (b) $\Delta n_2 = 0.5\Delta n_1$, and (c) $\Delta n_2 = 0.1\Delta n_1$ to result in the three corresponding plots. The data points designated by Δ and \circ were taken from the corresponding plots of Ref. [2] for comparison.

Table 1
Calculated diffraction efficiencies and errors for the four diffraction angles

Grating #	Diff. angle	N = 50		N = 100		N = 200	
		Efficiency %	Error %	Efficiency %	Error %	Efficiency %	Error %
1	−20°	26.06597	1.47	25.79094	0.74	25.65374	0.37
2	20°	25.68533		25.60165		25.55936	
3	−10°	24.15778	1.41	24.25333	0.70	24.30071	0.35
4	10°	23.81902		24.08295		24.21526	

second grating were set at $\Delta n_2 = \Delta n_1$, $\Delta n_2 = 0.5\Delta n_1$, and $\Delta n_2 = 0.1\Delta n_1$ to produce three sets of angular selectivity curves plotted in Fig. 3(a), 3(b), and 3(c), respectively. Our results match well to those calculated using the thin-grating decomposition technique [2]. The validity of our technique for analyzing Bragg diffractions by three or more superimposed transmission phase gratings with well separated Bragg angles is expected although the result comparison has not yet been performed due to the lack of published selectivity curves by other techniques.

To examine the behavior of Bragg diffractions by superimposed transmission phase gratings, a set of diffraction efficiencies for different diffracted beams were computed at different diffraction angles and grating index modulations. The following parameters were used for the calculation: bulk index $n_0 = 1.5$; incident-beam wavelength $\lambda = 632.8$ nm; incident angle $\alpha = 0^\circ$; four sets of diffracted beam angles and grating index modulations ($-20^\circ, 0.003$), ($-10^\circ, 0.003$), ($10^\circ, 0.003$) and ($20^\circ, 0.003$); and TE incident beam polarization. The total grating thickness was $50 \mu\text{m}$ and the numbers of partitioned grating subsections N (with equal subsection length) were 50, 100, and 200, respectively. The calculated diffraction efficiencies are listed in Table 1.

For symmetry diffractions ($\alpha = 0^\circ$ and same diffraction angles with opposite signs) the diffraction efficiencies are expected to be the same. The slight differences in efficiencies for diffraction angles at 20° and -20° are obviously N dependent. The larger the grating subsection number N , the smaller each grating subsection length and the smaller the efficiency computational error for the symmetric diffracted beams. The same argument holds for other symmetric diffraction angles at -10° and 10° . When N are 1000 and 10000, the computation for the above exam-

ple shows errors of only 0.074% and 0.0074%, respectively.

The computation error is not only N dependent. It depends on grating subsection length Δd , incident angle, diffraction angle, wavelength, and grating index modulation. In general, we should choose smaller $\Delta d = d/N$ (or larger N) under strong diffraction cases for better computational accuracy with a trade-off of longer computation time.

At a fixed diffraction geometry determined by application requirements, all the above diffraction parameters are fixed except the grating index modulations. To achieve uniform diffraction efficiencies for all diffracted beams for some fanout interconnect applications, the grating index modulations can be adjusted to establish a suitable combination of grating index modulations prior to device implementations. Since changing one grating index modulation can affect the diffraction efficiencies of all diffracted beams, the selection of a suitable combination of grating index modulations must be according to overall efficiency distributions. For diffracted beams with efficiencies over the expected average their grating index modulations must be adjusted in the decreasing efficiency direction. For diffracted beams with efficiencies lower than the expected average their grating index modulations must be adjusted in the increasing efficiency direction.

Table 2 shows a calculation example with incident beam wavelength of 632.8 nm, TE incident polarization, bulk grating index of 1.5, incident angle of 0° , total grating thickness of $50 \mu\text{m}$, and 10000 partitioned grating subsections. The diffraction efficiencies are not uniformly distributed with the identical index modulation of 0.003. After the grating index adjustment all four diffracted beams approach the expected average efficiency of 25%. Both

Table 2
Example of grating index adjustment for better efficiency uniformity

Grating #	Diff. angle	Before index adjustment		After index adjustment	
		Index mod.	Efficiency %	Index mod.	Efficiency %
1	20°	0.003	20.70959	0.00342	24.29295
2	30°	0.003	22.46939	0.00327	24.09536
3	40°	0.003	25.39970	0.00308	24.16410
4	50°	0.003	30.26699	0.00283	24.30990

index modulations for gratings 1 and 2 are increased since the original efficiencies were lower than the expected average. The index modulation for grating 4 is decreased since the original efficiency was higher than the expected average. The efficiency for grating 3 was most closed to the expected efficiency. Its index adjustment is based on the outcome of other grating index adjustments that affect its efficiency. In theory, we can achieve exactly 25% for all diffracted beams of the present example by index adjustment. Further index adjustment was not attempted owing to the practical concern on the significant digits of the grating index modulation. It should be possible to establish a computation algorithm to adjust the grating index modulations and provide reasonably uniform diffraction efficiencies for all diffracted beams. Establishing correct combinations of grating index modulations can make device implementation a lot easier.

4. Dephasing effects and angular and wavelength selectivities

Angular and wavelength selectivities are important figures of merit for phase grating-based devices. Diffractions by superimposed transmission phase gratings with significant energy coupling among all diffracted and undiffracted beams are expected to affect the selectivity features. Here the angular and wavelength selectivities are examined to show their departures from the single-grating diffractions.

For a fixed incident angle α , a set of diffracted angles α_d , and center wavelength, the wavelength selectivities can be calculated through the wavelength dependent changes in the dephasing constant ϑ . The calculations indicate a strong dependence of dephasing and wavelength selectivity on the grating index modulations Δn and the diffraction angles α_d .

Fig. 4(a) and Fig. 4(b) show wavelength-selectivity plots for the example of Table 2 before and after the grating index adjustment, respectively. Each grating subsection length is only $0.005 \mu\text{m}$ and we observe no significant difference on the sequence of the grating diffraction in each subsection. The selectivity curves appear to depart significantly from the $(\text{sinc})^2$ functional dependence of the single grating diffraction case [9,14]. There are changes in central selectivity curves, selectivity bandwidths, and side-lobe features. For the largest diffraction angle, the changes in side-lobe maxima and minima are those which appear most. For the smallest diffraction angle, the most significant changes appear near the central selectivity curve. These behaviors are believed to be caused by the energy coupling among all diffracted and undiffracted beams with different original single-grating selectivity bandwidths. For larger diffraction angles, their single-grating selectivity bandwidths are smaller while for smaller diffraction angles their single-grating selectivity bandwidths are larger. Thus, in the superimposed grating diffraction case the largest-angle diffraction is affected

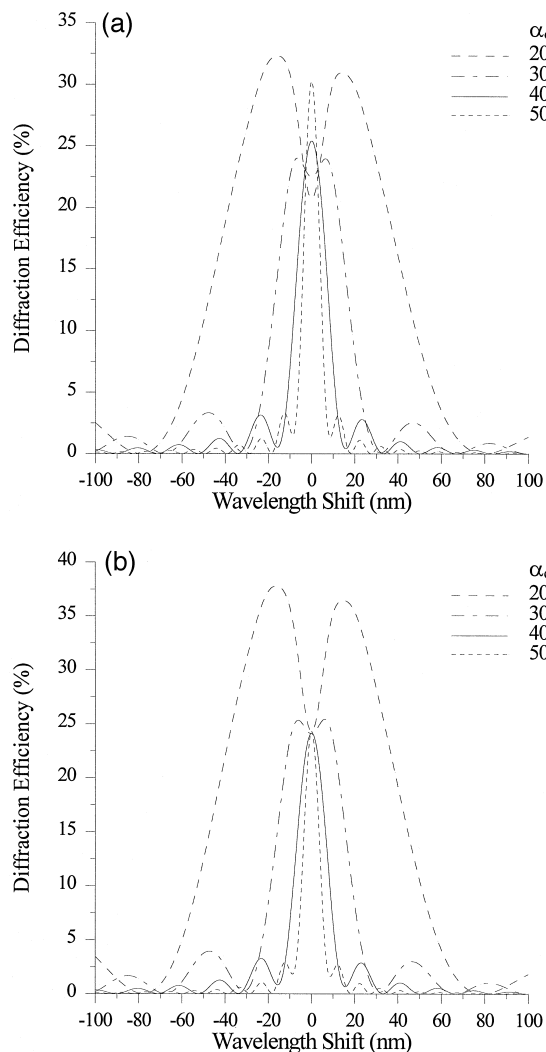


Fig. 4. Calculated wavelength selectivity curves for the superimposed grating diffractions of Table 2 (a) before and (b) after the grating index adjustment.

mostly in its side-lobe features by the smaller-angle diffractions. The smallest-angle diffraction is affected the most in its central selectivity curve by the larger-angle diffractions. The diffractions with other angles appear to have changes in both central selectivity curves and side-lobe features. The degree of the changes in central selectivity curves or side-lobe features depends on how close they are to the smallest or the largest diffraction angle and the coupling strength of other gratings. As the wavelength shifted slightly away from the Bragg condition in this case, the diffraction efficiency of the largest diffraction angle decreases while the diffraction efficiency of the smallest diffraction angle increases. The increasing or decreasing of the efficiencies of other diffracted beams depends on the superimposed grating diffraction situations. Further wavelength shifts away from the Bragg condition result in

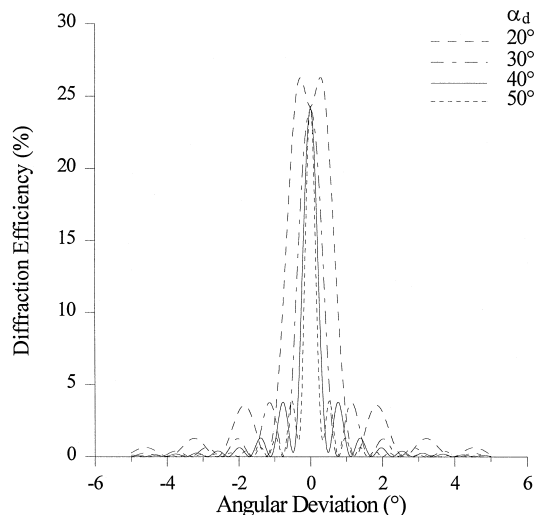


Fig. 5. Angular selectivity plots for the superimposed grating diffractions of Table 2 after the grating adjustment.

non-diffraction at the largest diffraction angle first, then the second largest diffraction angle, and so on, and eventually non-diffraction at the smallest diffraction angle. The small grating index adjustment for achieving uniform fanout diffraction efficiencies affects mostly the central efficiency curves.

Fig. 5 shows the calculated angular selectivity curves for the example of Fig. 4(b). Incident beam wavelength is now fixed while the incident beam angle is allowed to vary slightly from the designed direction. Again, similar to the plot of Fig. 4(b), the angular selectivity curve shows significant departure from the $(\text{sinc})^2$ functional dependence with significant changes in side-lobe features at the largest diffraction angle and significant changes in the central selectivity curve at the smallest diffraction angle. Again a slight angular deviation from the Bragg condition decreases the diffraction efficiency at the largest diffraction angle and increases the efficiency at the smallest diffraction angle in this case. In general, the effects of the angular deviation to the superimposed grating diffraction efficiencies at different diffraction angles are similar to the wavelength-selectivity plots of Fig. 4(b) because they are both derived through the dephasing factor ϑ .

5. Polarization effects

The computation technique described in this paper can apply to both TE and TM incident beams with different coupling constants given in Eq. (6). Any incident beam polarization can be decomposed into TE and TM components and then we calculate their diffracted beam field amplitudes separately. The resulting diffracted beams with both TE and TM field amplitudes can then be used to evaluate their final polarizations. In general, a linearly

polarized incident beam with its polarization direction not in the incident plane or perpendicular to the incident plane will result in different elliptical polarized output diffracted beams at different diffraction angles. This is caused by the different grating coupling strengths for TE and TM polarized beams that in term result in different energy distribution for these two polarizations in the diffracted beam directions. With non-polarized incident beam, the polarization effect should be considered along with the grating adjustment to achieve the required fanout energy distributions.

6. Conclusions

In summary, a simple numerical computation technique is described for the analysis of Bragg diffractions by superimposed transmission phase gratings. The thin grating sequential diffraction technique is useful for treating any number of superimposed transmission phase gratings with both symmetric and asymmetric diffraction geometries. The wavelength and angular selectivity curves are observed to depart from the $(\text{sinc})^2$ functional dependence of single-grating diffractions. The selectivity features of a particular diffracted beam are found to depend on other superimposed gratings. Any change in one grating index modulation will affect the overall diffracted beam energy distributions. Therefore, obtaining correct grating index combinations prior to device implementation is expected to reduce significantly the experimental efforts. The technique should prove valuable for the design and optimization of optical beam splitters based on the superimposed phase grating diffractions.

References

- [1] R. Alferness, *Appl. Phys.* 7 (1975) 29.
- [2] R. Alferness, S.K. Case, *J. Opt. Soc. Am.* 65 (1975) 730.
- [3] S.K. Case, *J. Opt. Soc. Am.* 65 (1975) 724.
- [4] V. Minier, A. Kevorkian, J.M. Xu, *IEEE Photonics Technol. Lett.* 4 (1992) 1115.
- [5] R. Kowarschik, *Optica Acta* 25 (1978) 67.
- [6] E.N. Glytsis, T.K. Gaylord, *Appl. Optics* 28 (1989) 2401.
- [7] R. Magnusson, T.K. Gaylord, *J. Opt. Soc. Am.* 67 (1977) 1165.
- [8] M.G. Moharam, T.K. Gaylord, *J. Opt. Soc. Am.* 73 (1983) 1105.
- [9] M.R. Wang, G.J. Sonek, R.T. Chen, T. Jansson, *Appl. Optics* 31 (1992) 236.
- [10] K.Y. Tu, T. Tamir, *Appl. Optics* 32 (1993) 3654.
- [11] K.Y. Tu, T. Tamir, H. Lee, *J. Opt. Soc. Am. A* 7 (1990) 1421.
- [12] S. Ahmed, E.N. Glytsis, *Appl. Optics* 35 (1996) 4426.
- [13] P. Asthana, G.P. Nordin, A.R. Tanguay Jr., B.K. Jenkins, *Appl. Optics* 32 (1993) 1441.
- [14] H. Kogelnik, *Bell Syst. Technol. J.* 48 (1969) 2909.
- [15] M.R. Wang, *Appl. Optics* 35 (1996) 582.